Multi-Rate Mass Transfer (MRMT) models for general diffusive porosity structures

Tristan Babey, Jean-Raynald de Dreuzy, Céline Casenave

Multi-Rate Mass Transfer (MRMT) models for general diffusive porosity structures

Tristan Babey[1], Jean-Raynald de Dreuzy[1], Céline Casenave[2,3]

[1]Géosciences Rennes (UMR CNRS 6118), Campus de Beaulieu, Université de Rennes 1, 35042 Rennes cedex, France

[2]UMR INRA-SupAgro 0729 MISTEA, 2 place Viala 34060 Montpellier, France

[3]MODEMIC project-team, INRA/INRIA, Sophia-Antipolis, France

Corresponding author: Tristan Babey, +33646204318, tristan.babey@univ-rennes1.fr

Highlights:

- A mobile-immobile transport model with a structured immobile domain is proposed
- Structured INteracting Continua-SINC generalize Multiple INteracting Continua-MINC
- Whatever the SINC structure, a unique equivalent MRMT model exists
- MRMT models with only very few rates accurately model conservative transport
- We propose a robust numerical identification of the first few rates

ABSTRACT

We determine the relevance of Multi-Rate Mass Tansfer (MRMT) models to general diffusive porosity structures. To this end, we introduce Structured INteracting Continua models (SINC) as the combination of a finite number of diffusion-dominated interconnected immobile zones exchanging with an advection-dominated mobile domain. It directly extends Multiple INteracting Continua framework [*Pruess and Narasimhan*, 1985] by introducing a structure in the immobile domain, coming for example from the dead-ends of fracture clusters or poorly-connected dissolution patterns. We demonstrate that, whatever their structure, SINC models can be made equivalent in terms of concentration in the mobile zone to a unique Multi-Rate Mass Transfer (MRMT) model [*Haggerty and Gorelick*, 1995]. We develop effective shape-free numerical methods to identify its few dominant rates, that comply with any distribution of rates and porosities. We show that differences in terms of macrodispersion are not larger than 50% for approximate MRMT models with only one rate (double porosity models), and drop down to less than 0.1% for five rates MRMT models. Low-dimensional MRMT models

accurately approach transport in structured diffusive porosities at intermediate and long times and only miss early responses.

Keywords: Porous media; Solute transport; Mobile-immobile models; Multi-Rate Mass Transfer;

1 Introduction

Transport in complex geological environments results in part from the interactions between fast advective-dominated transport in a localized "mobile porosity" and slow diffusive-dominated transport in extensive "immobile porosities". It is the case of the fracture-matrix systems [*Neretnieks*, 1980; *Tang et al.*, 1981] and of the highly heterogeneous porous media [*Fernandez-Garcia et al.*, 2009; *Golfier et al.*, 2007; *Gotovac et al.*, 2009; *Willmann et al.*, 2008]. When diffusive times in the immobile zones become much larger than the characteristic advective time in the mobile zone, transport becomes anomalous with non-Gaussian concentration plumes, more extensive spreading and mixing, slow transit times, and broad ranges of solute retardation times [*Berkowitz et al.*, 2006; *Dentz et al.*, 2004]. Such transport mechanisms and exchanges are at the root of numerous anomalous transport modeling frameworks [*Benson and Meerschaert*, 2009; *Benson et al.*, 2000; *Berkowitz and Scher*, 1998; *Carrera et al.*, 1998; *Cushman and Ginn*, 2000; *Haggerty and Gorelick*, 1995] and can be highly effective in the interpretative and predictive phases of laboratory and field experiments [*Benson et al.*, 2001; *Berkowitz et al.*, 2000; *Gouze et al.*, 2008; *Haggerty et al.*, 2001; *Haggerty et al.*, 2004]. Anomalous transport ultimately stems from some extended distribution whether it is a waiting time distribution as in Continuous Time Random Walk (CTRW) or a rate-porosity distribution as in Mutli-Rate Mass Transfert (MRMT) [*Dentz and Berkowitz*, 2003; *Neuman and Tartakovsky*, 2009; *Silva et al.*, 2009]. For MRMT models, while these distributions can take very different shapes [*Haggerty et al.*, 2000], only some power-law distributions are effectively related to diffusive processes in 1D, 2D or 3D inclusions [*Carrera et al.*, 1998; *Haggerty and Gorelick*, 1995] or to anomalous diffusive processes in fractal-like structures [*Haggerty*, 2001]. Diffusive structures may however be topologically more complex like for example for fracture dead ends [*Flekkøy et al.*, 2002; *Sornette et al.*, 1993], fracture-matrix interactions [*Jardine et al.*, 1999; *Karimi-Fard et al.*, 2006; *Sudicky and Frind*, 1982; *Tang et al.*, 1981; *Tsang*, 1995], or dissolution patterns in porous media [*Golfier et al.*, 2002; *Luquot et al.*, 2014] (Figure 1).

In this article, we show that the MRMT framework is general to all diffusive architectures that can be modeled as a finite number of interconnected continua (Figure 1). The notion of continuum comes from the double porosity and Multiple INteracting Continua (MINC) concepts introduced initially for fracture-matrix systems [*Pruess and Narasimhan*, 1985; *Warren et al.*, 1963]. The double porosity model is the classical diffusive interaction of advective-diffusive processes in a mobile zone with a single immobile zone like in double-

porosity models [*Warren et al.*, 1963]. The Multiple INteracting Continua (MINC) framework models matrix diffusion as diffusive-like exchanges within a succession of "continua", identified to the elementary cells issued by a finite-difference discretization of the diffusion process in the matrix (Figure 2a) [*Pruess*, 1992; *Pruess and Narasimhan*, 1985]. The denomination of multiple continua is a direct generalization of the double porosity concept of *Warren and Root* [1963]. We propose to further generalize the notion of interacting continua to any immobile zones structure where diffusive-like exchanges intervene between any connected zones or continua. Because of the potential importance of structure on diffusion, we denote these models as Structured INteracting Continua (SINC). SINC models include a wide range of structures going from elementary branching and loops (Figure 2b and c) to more involved dissolution patterns (Figure 2d). They would typically be derived from the coarse discretization of diffusion processes in dead-end porosity structures [*Gouze et al.*, 2008; *Noetinger and Estebenet*, 2000]. We define SINC models in section 2, with their exact relation to the MRMT and MINC models. We show in section 3 that any SINC model is equivalent in terms of transport to a unique MRMT model of the same dimension, i.e. with the same number of immobile zones. We develop efficient numerical methods in section 4 to identify lower-dimension but highly accurate approximate MRMT models.

(a) Limestone dissolution structure [*Luquot et al.*, 2014]	(b) SINC model	(c) Equivalent MRMT model
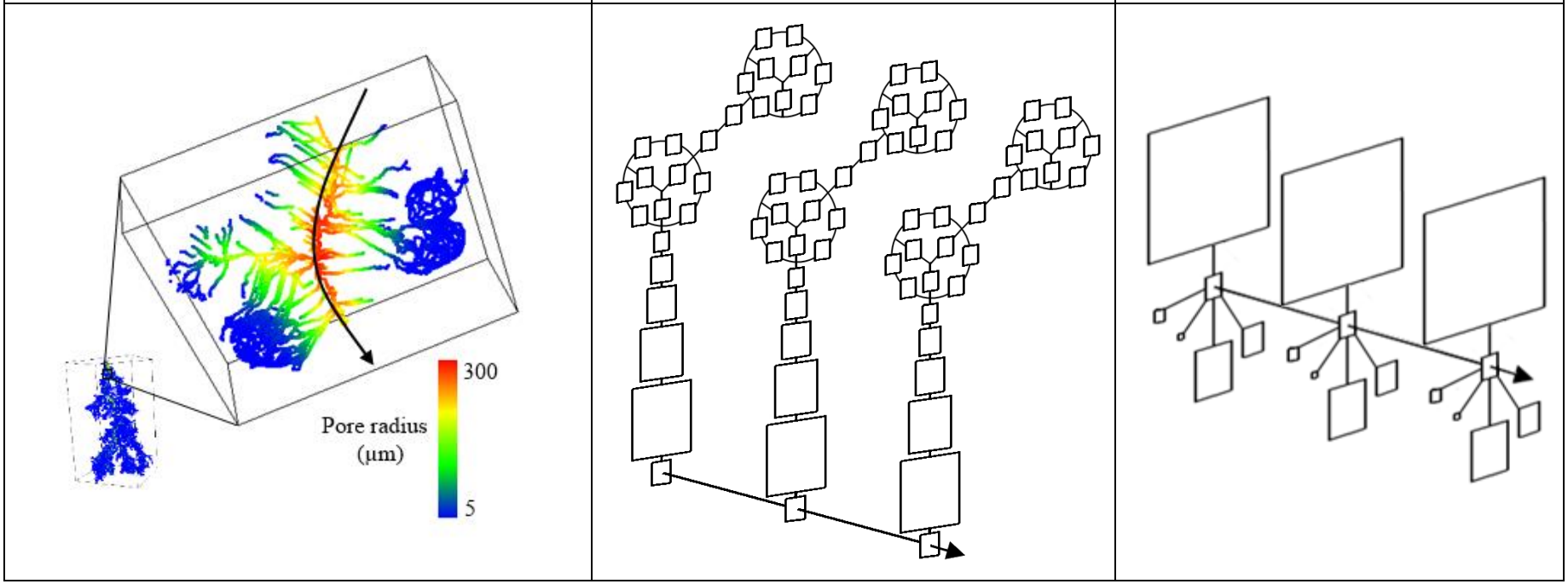		

Figure 1: (a) Skeleton of a dissolution feature in an oolitic limestone, observed by X-ray micro-tomography [*Luquot et al.*, 2014]. The dissolving acidic solution percolates from top to bottom on the general view (bottom left). Its pH increases from top to bottom and from inside out of the main flow path indicated by the curved arrow on the detailed view (top right). The acid dissolves preferentially the calcite cement surrounding the oolites, the size of the pores progressively decreases away from the main flow path, and the organization of the pores becomes more complex. (b) Structured INteracting Continua model (SINC) sketched from the dissolution pattern of (a) with three cross sections transversal to the mobile zone materialized by the arrow. (c) Equivalent MRMT model with the 5 most important rates as determined by the numerical methods set up in section 4. The size of the boxes scales with the porosity affected to the rates labeled by triangles in Figure 7.

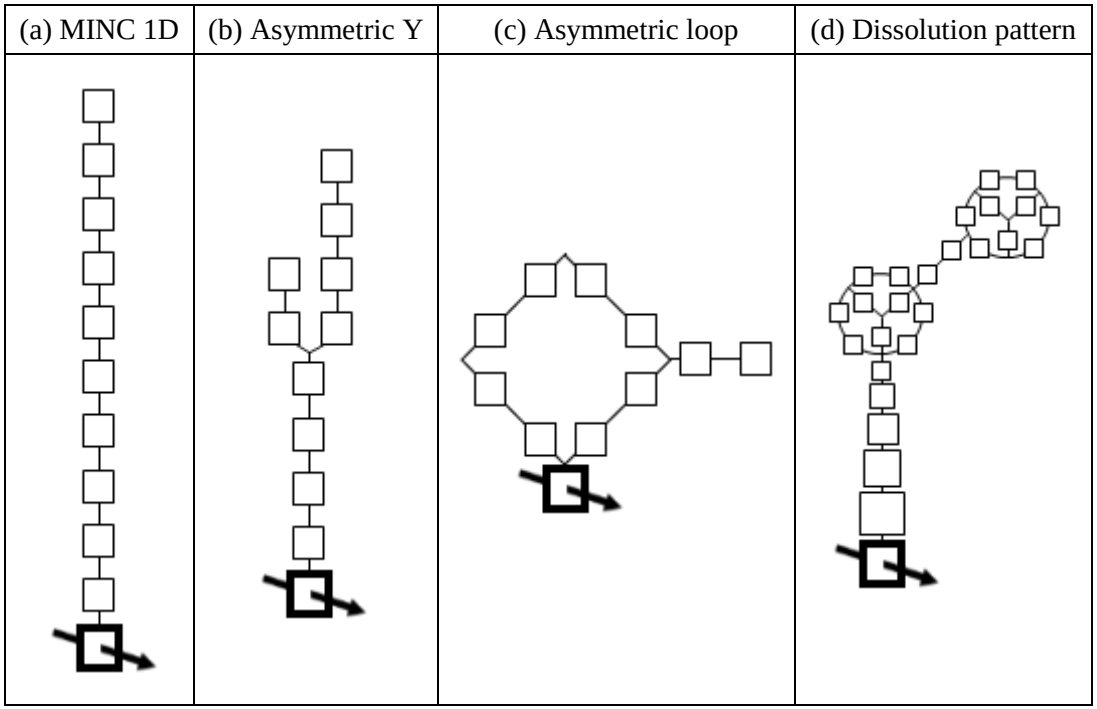

Figure 2: Examples of Structured INteracting Continua (SINC) used to illustrate and validate the numerical identification methods of the equivalent MRMT models. From left to right, the diffusive porosity structures are (a) the classical Multiple INteracting Continua (MINC) [*Pruess and Narasimhan*, 1985], (b) an asymmetric Y with a single junction, (c) an asymmetric loop, and (d) the dissolution structure presented in Figure 1. The size of the immobile cells is proportional to their porosity and the distance along the immobile structure is to scale. The mobile zone is represented by the thick black box with the crossing arrow. Its size has been exaggerated 10 times to be clearly marked. To be comparable, the four structures have the same total porous volume and the same radius of gyration taken with respect to the mobile zone.

2 Structured INteracting Continua (SINC)

We present the Structured INteracting Continua framework (SINC) and show how it relates to existing models like Multi-Rate Mass Transfer (MRMT) and Multiple INteracting Continua (MINC).

The SINC model is made up of a continuous 1-D mobile zone in interaction with a finite number of interconnected immobile zones (Figure 1). In the continuous mobile zone, solutes are transported by advection, dispersion and diffusion. Between the mobile zone and the immobile zones as well as between the immobile zones, concentration exchanges are diffusive-like, i.e. directly proportional to the difference of concentrations. This model can be generically expressed as:

$$\frac{\partial U}{\partial t} - AU = L(R_m U) \tag{1}$$

where $U = [c_m(x,t) \quad c_{im}^1(x,t) \quad \cdots \quad c_{im}^N(x,t)]^T$ is the vector of dimension N+1 made up of the concentrations in the mobile zone $c_m(x,t)$ and in the N immobile zones $c_{im}^i(x,t)$ with $i = 1,\ldots,N$. A is the $(N+1, N+1)$ interaction matrix characterizing the diffusive-like concentration exchanges between the immobile zones and with the mobile zone. R_m is the restriction matrix to the mobile zone:

$$R_m(i, j) = \delta(i-1)\delta(j-1). \tag{2}$$

L is the transport operator in the mobile zone:

$$L(c_m) = -\frac{q}{\phi_m}\frac{\partial c_m}{\partial x} + d_m \frac{\partial^2 c_m}{\partial x^2} \tag{3}$$

with q, ϕ_m and d_m the Darcy flow, porosity and dispersion coefficient in the mobile zone. The physical properties of the mobile and immobile domains are homogeneous along the mobile domain. The interaction matrix A is equal to the matrix M deriving from the diffusive-like mass exchanges between the different zones, corrected by their porosities:

$$A = -\Phi^{-1} M \tag{4}$$

with Φ the diagonal matrix whose diagonal elements are the porosities associated to the mobile zone ϕ_m and to the N immobile zones ϕ_{im}^i with $i = 1,\ldots,N$:

$$\begin{cases} \Phi(1,1) = \phi_m \\ \Phi(i,j) = \phi_{im}^{i-1}\delta(i,j) \quad \text{for } (i,j) \neq (1,1) \end{cases}. \tag{5}$$

The matrix M expresses rates of mass exchange. The dimension of its elements is therefore the inverse of a time. As exchanges are diffusive-like, M is a M-matrix, i.e. M is symmetric, its diagonal elements are positive, its off-diagonal elements are negative or equal to zero, and the sum of its elements along each of its rows is equal to zero. We underline that it is the matrix M that is symmetric and generally not the interaction matrix A that also integrates the differences in porosities. The interaction matrix A registers the connectivity of the different zones through the position of its non-zero off-diagonal elements, the strength of the interactions is determined by porosity ratios and exchange rates. Figure 3a shows the example of the interaction matrix for the asymmetric Y structure (cf Figure 2b). The branching architecture leads to a compact interaction matrix, which values are all on the three principal diagonals except at the branching node. The interaction matrix is scaled by the inverse of the mean diffusion time in the immobile structure τ. We define τ as the quadratic mean distance of the immobile zones to the mobile zone divided by the diffusion coefficient between two zones.

The SINC framework generalizes Multiple INteracting Continua (MINC) [*Pruess and Narasimhan*, 1985]. MINC models are obtained by the finite-difference discretization of diffusion in a 1-D homogeneous medium. In such a case, the interaction matrix A is simply tri-diagonal. The term "continuum" comes from the continuity along the mobile zone like in the dual-porosity concept [*Warren et al.*, 1963]. It is consistent with our concept of a continuous formalism of transport along the mobile zone and a finite number of interacting continua in the immobile direction.

The SINC framework also generalizes Multiple-Rate Mass Transfer models with a finite number of rates [*Carrera et al.*, 1998; *Haggerty and Gorelick*, 1995]. In MRMT models as defined by *Haggerty et al.* [1995], the immobile domain consists in a distribution of sub-domains exchanging exclusively with the mobile domain. The star-like connectivity structure leads to an arrow-type broad-width interaction matrix (Figure 3b). Each sub-domain is characterized by its rate of transfer α_i and its porosity ϕ_{im}^i, with $\alpha_i < \alpha_{i+1}$ [*Haggerty and*

149 *Gorelick*, 1995]. When defined with a finite number of rates, MRMT models can be recovered
150 by fixing

$$\begin{cases} M(i,j)=0 \quad \text{for } i>1,\ j>1 \text{ and } i\neq j \\ M(i,1)=M(1,i)=-\phi_{im}^{i-1}\alpha_{i-1} \quad \text{for } i>1 \\ M(i,i)=-\sum_{j,j\neq i} M(i,j) \end{cases} . \qquad (6)$$
$$\begin{cases} \Phi(1,1)=\phi_m \\ \Phi(i,j)=\phi_{im}^{i-1}\delta(i,j) \quad \text{for } (i,j)\neq(1,1) \end{cases}$$

151 Because they are defined in algebraic terms, SINC models can only represent MRMT models
152 with finite number of rates. They are rigorously not equivalent to 1D, 2D and 3D diffusion
153 models that themselves correspond to an infinite number of exchange rates [*Haggerty and*
154 *Gorelick*, 1995]. However they offer very accurate approximations when taking only a finite
155 number of rates, especially as the porosities ϕ_{im}^{i} decrease as a power law of *i*. SINC models
156 generalize MRMT models defined with a finite number of rates but remain different to
157 MRMT models defined by an infinite serie of rates or by a continuous rate-porosity function.
158 Our objective in this article is not to produce any kind of generalization of MRMT models but
159 rather to determine how complex diffusive porosity structures can be approached by simpler
160 reduced models.

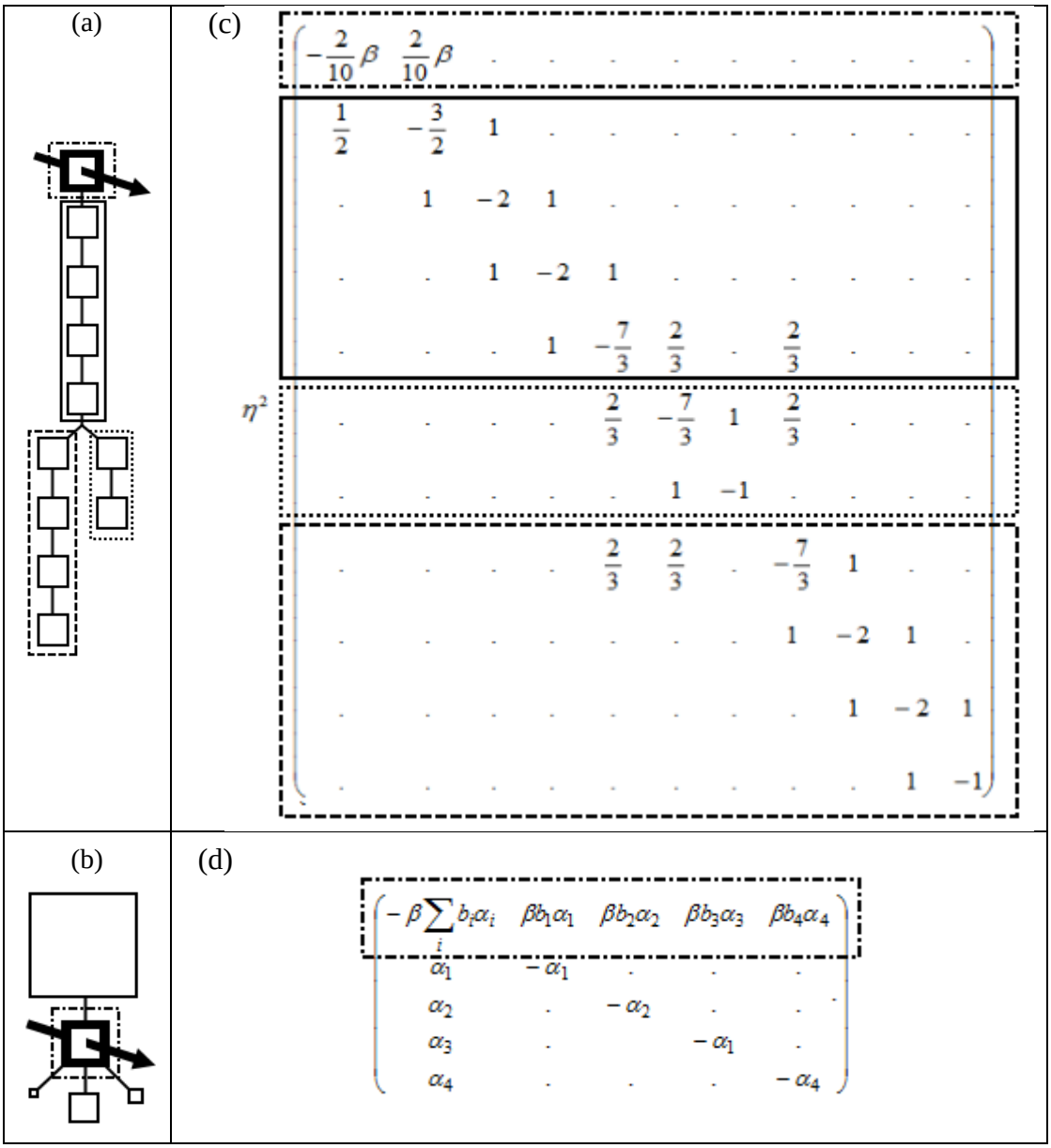

Figure 3: Diffusive porosity structures represented as cross-sections transversal to the mobile zone direction ((a),(b)), with their associated interaction matrix *A* ((c),(d)) for the asymmetric Y (*top*) and MRMT structures (*bottom*). Dotted frames around subsets of the immobile porosity structures ((a) and (b)) and around matrix lines ((c) and (d)) show how structures are translated in matrix form. Parameters for the asymmetric Y structure are taken from Table 1 and the multiplicative factor η (η=5.015) is equal to the ratio of the distance between two consecutive immobile zones to the radius of gyration of the immobile domain to the mobile zone. β is the ratio of the total immobile porosity to the mobile porosity.

3 Proof of equivalence of SINC to MRMT model

Following up the work of *Haggerty and Gorelick* [1995], we define the equivalence relation to a MRMT model as the identity of the mobile concentration at any time. To prove the equivalence of the SINC model to a MRMT model, we first decompose the interaction matrix A in two parts, consisting in the exchanges between the immobile zones only for the first part and in the exchanges between the mobile zone and the immobile zones for the second one:

$$A = \begin{pmatrix} 0 & \cdots & \cdots & 0 \\ \vdots & & & \\ \vdots & & \widehat{A} & \\ 0 & & & \end{pmatrix} + \begin{pmatrix} A_{11} & A_{12} & \cdots & A_{1,N+1} \\ A_{21} & & & \\ \vdots & & 0 & \\ A_{N+1,1} & & & \end{pmatrix} \tag{7}$$

with $\widehat{A} = A(2 \ldots N+1, 2 \ldots N+1)$. As shown in *Appendix A*, the matrix $\widehat{A}$ can be diagonalized

$$\widehat{A} = \widehat{R} \Lambda \widehat{R}^{-1} \tag{8}$$

with Λ the diagonal matrix made up of the eigenvalues of $\widehat{A}$, which are all real and negative, and $\widehat{R}$ the matrix of the eigenvectors of $\widehat{A}$, defined each up to a multiplicative constant. To fix the eigenvalues decomposition, as Λ is defined up to a permutation of its diagonal elements, we sort the eigenvalues according to their absolute value by increasing order $\left|\Lambda_{i,i}\right| \leq \left|\Lambda_{i+1,i+1}\right|$. In the new coordinate system defined by the eigenvectors, there are no more exchanges between the immobile zones. All exchanges are made directly between the immobile zones and the mobile zone. To characterize the precise nature and extent of these exchanges, we propagate the change of the coordinate system to the exchanges with the mobile zone

$$\begin{pmatrix} A_{11} & A_{12} & \cdots & A_{1,N+1} \\ A_{21} & & & \\ \vdots & & 0 & \\ A_{N+1,1} & & & \end{pmatrix} = R \begin{pmatrix} A_{11} & B_{12} & \cdots & B_{1,N+1} \\ B_{21} & & & \\ \vdots & & 0 & \\ B_{N+1,1} & & & \end{pmatrix} R^{-1} \tag{9}$$

with the $(N+1, N+1)$ matrix R and its inverse R^{-1} defined as

$$R = \begin{pmatrix} 1 & 0 & \cdots & 0 \\ 0 & & & \\ \vdots & & \widehat{R} & \\ 0 & & & \end{pmatrix} \text{ and } R^{-1} = \begin{pmatrix} 1 & 0 & \cdots & 0 \\ 0 & & & \\ \vdots & & \widehat{R}^{-1} & \\ 0 & & & \end{pmatrix}. \tag{10}$$

In this transformation, the mobile zone remains unchanged consistently with our objective to reorganize only the immobile zones without interfering with the concentration in the mobile zone. The full transformation defined by R is applied to the matrix A following its decomposition in equation (7)

$$A = R \begin{pmatrix} 0 & \cdots & \cdots & 0 \\ \vdots & & & \\ \vdots & & \Lambda & \\ 0 & & & \end{pmatrix} R^{-1} + R \begin{pmatrix} A_{11} & B_{12} & \cdots & B_{1,N+1} \\ B_{21} & & & \\ \vdots & & 0 & \\ B_{N+1,1} & & & \end{pmatrix} R^{-1} \tag{11}$$

which can be finally expressed by a simple factorization as

$$A = RBR^{-1} \text{ with } B = \begin{pmatrix} A_{11} & B_{12} & \cdots & B_{1,N+1} \\ B_{21} & & & \\ \vdots & & \Lambda & \\ B_{N+1,1} & & & \end{pmatrix}. \tag{12}$$

Finally, as the restriction matrix to the mobile zone R_m (equation (2)) commutes with R^{-1}, we can write the full model as

$$\frac{\partial R^{-1}U}{\partial t} - BR^{-1}U = L\left(R_m R^{-1}U\right). \tag{13}$$

To be representative of a MRMT model, B should be an arrow matrix, the sum of its elements over each of its rows should be zero, and all its non-diagonal elements must be either positive or equal to zero. In *Appendix B*, we show that this can be obtained by adjusting the norm of the eigenvectors in $\widehat{R}$. The characteristics of this MRMT model are then determined by a simple identification of equation (6) with equation (12):

$$\begin{cases} \alpha_i = -\Lambda_i \\ \phi_{im}^i = \phi_m \dfrac{B_{1,i+1}}{B_{i+1,1}} = \phi_m \dfrac{B_{1,i+1}}{-\Lambda_i} \end{cases} \quad (14)$$

While this algebraic identification method can already be widely used to determine equivalent MRMT models, it faces some numerical limitations. The diagonalization process becomes challenging when $\hat{A}$ becomes large, limiting the range of the identification to not too complex architectures and/or coarse discretizations of the immobile domain. The immobile porosity structure may be composed of a large number of cells, while a much smaller number of rates may be necessary to get highly accurate equivalent MRMT models. To address these limitations, we propose an alternative approximate numerical identification method.

4 Approximate numerical identification method of the MRMT model equivalent to a SINC model

We first develop the numerical methodology and secondly apply it to the four examples of Figure 2. Because of their widely differing structures, these four SINC examples are thought to be a good basis for testing and illustrating the numerical methods. The first one is the classical MINC taken as reference. The two next ones were chosen for their elementary branching and looping connectivity patterns (Figure 2b and c). Any more involved patterns like the dissolution pattern of Figure 2d will be some kind of combination of these elementary structures. These four examples are comparable in the sense that they have the same mobile properties, the same overall immobile to mobile porosity ratio β, and the same mean quadratic diffusion time τ as defined in section 2 (Table 1). The dispersivity in the mobile zone $d_m \bar{l}(q/\phi_m)$ divided by the effective dispersivity due to the exchanges with the immobile zone defined as $\tau(q/\phi_m)$ is taken equal to 5.10^{-5}, i.e. much smaller than 1, so that dispersive effects come predominantly from the mobile/immobile exchanges. For the same reason, β is taken much larger than 1 ($\beta = 100$).

Parameter	Value
β	100
$d_m/\left(\tau\left(q/\phi_m\right)^2\right)$	5.10^{-5}
$\sigma_0/\left(q\tau/\phi_m\right)$	3.10^{-3}
$x_{\max}/\sigma_0$	100
dx/σ_0	0.2
dt/τ	5.10^{-4}

Table 1: Parameters used for the simulation of section 4.2 with the characteristic diffusion time τ and the consecutive distance covered by advection in the mobile zone $q\tau/\phi_m$ as temporal and spatial dimensional parameters. β is the immobile to mobile porosity ratio. $d_m/\left(\tau\left(q/\phi_m\right)^2\right)$ is the dimensionless dispersion in the mobile zone. $\sigma_0/\left(q\tau/\phi_m\right)$ is the dimensionless standard deviation of the initial Gaussian concentration profile. $x_{\max}$ is the extension of the simulation domain in the direction of the mobile zone, *dx* is the spatial step along the mobile zone and *dt* is the time step.

4.1 Methodology

To numerically approximate the MRMT model equivalent to a SINC model, we consider the particular case of the discharge of the immobile zones to the mobile zone. The mass discharged to the mobile zone from an initially homogeneous immobile concentrations c_0 is fitted by a combination of exponential functions typical of the MRMT model. The residual mass per unitary volume $m(t)$ in the immobile domains is fitted by its MRMT counterpart $\gamma(t)$ given by:

$$\gamma(t) = \sum_{i=1}^{N} c_0 \phi_{im}^i \exp(-\alpha_i t) \tag{15}$$

where α_i and ϕ_{im}^i, $i = 1 \ldots N$ are the N rates and immobile porosities defined in equation (6). In *Appendix C*, we develop an optimization method to identify the α and ϕ_{im} series. We further illustrate its application to the cases $N = 1$ and $N = 2$ in *Appendix D*.

The advantage of this method over the previous algebraic method is to be flexible in terms of the number of rates N to identify. It also prioritizes the identification of the rates and immobile porosities having a significant impact on transport. In the following we determine the number of rates that should be identified to model accurately macrodispersive processes.

4.2 Simulations and results

We analyze the influence of the number of rates N on the reproduction of macrodispersion for the four structures displayed in Figure 2 for N ranging from 1 to 5. Identification is performed according to the methodology presented before and with a logarithmic sampling of times starting at the time for which the relative mass discharge to the mobile zone is lower than 10^{-3} and ending at the time for which the relative residual mass itself is lower than 10^{-4}.

Simulations of transport for the SINC and approximate MRMT models are further performed with identical Gaussian concentration profiles in the mobile and immobile domains

$$c_m(x, t=0) = c_{im}(x, t=0) = \frac{c_{\max}}{\sigma_0 \sqrt{2\pi}} \exp\left(-\frac{(x - x_0)^2}{2\sigma_0^2} \right) \tag{16}$$

where x_0, σ_0 and $c_{\max}$ are the mean, standard deviation and maximum concentration of the Gaussian profile. σ_0 is taken small enough so that the initial plume size has minor effects on the overall dispersion (Table 1).

252 We compute for all models the effective dispersion coefficient *D* as

$$D = \frac{1}{2}\frac{d\sigma_x^2}{dt} \tag{17}$$

253 with σ_x the plume spreading

$$\sigma_x^2 = m_2 / m_0 - (m_1 / m_0)^2 . \tag{18}$$

254 The spatial moments of concentration m_k are given by

$$m_k(t) = \int_{x=0}^{\infty} \sum_{i=1}^{N+1} x^k \Phi(i,i) U(x,t,i) dx . \tag{19}$$

255 We assess the quality of the MRMT model for modeling dispersion through the quadratic
256 mean of the relative difference in effective dispersion of the SINC and MRMT models:

$$diff(D_{SINC}, D_{MRMT}) = \sqrt{\int_t \left[\frac{D_{SINC}(t) - D_{MRMT}(t)}{(D_{SINC}(t) + D_{MRMT}(t))/2} \right]^2 dt \Big/ \int_t dt} . \tag{20}$$

257 This criterion is sensitive to differences in dispersion on a broad time range from the initial
258 time to the time at which dispersion becomes constant.

259 Classical numerical methods were used to solve both the exchanges within the immobile
260 zones and the advective-dispersive transport in the mobile zone [*de Dreuzy et al.*, 2013]. They
261 were validated on a set of immobile structures rigorously equivalent to the MINC model
262 (Figure 4). In those cases, $diff(D_{SINC}, D_{MINC})$ was of the order of 10^{-11} and much smaller than
263 any differences recorded in the analysis performed hereafter.

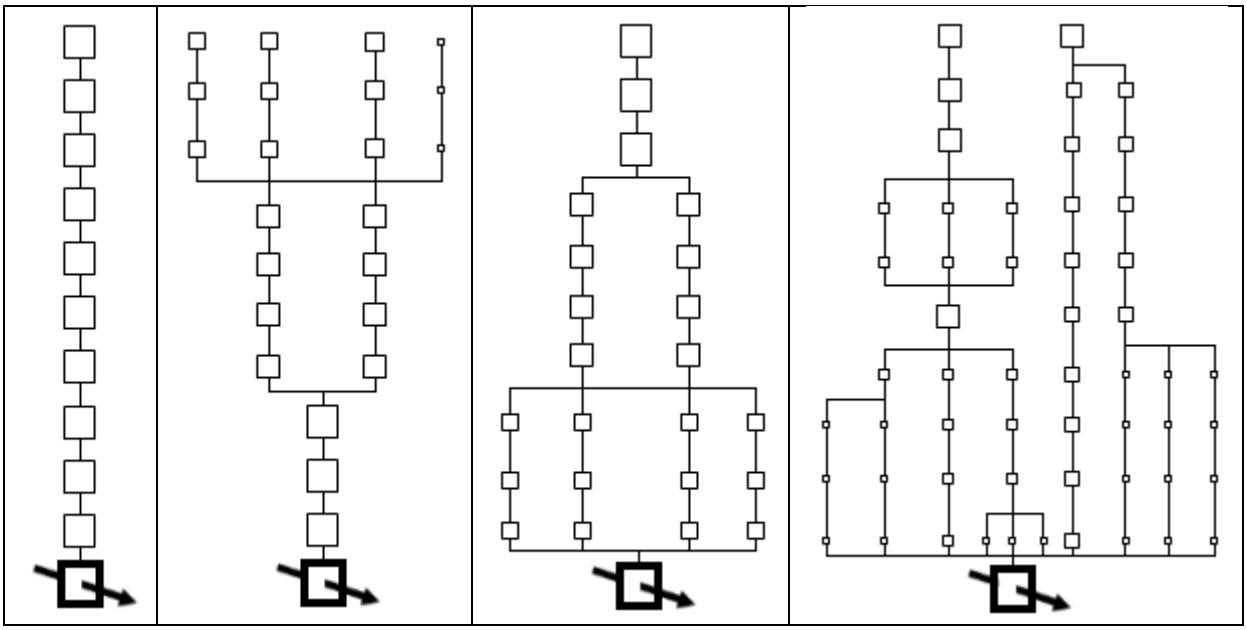

Figure 4: Diffusive porosity structures used to check the numerical implementation of the SINC model, equivalent to the "MINC 1D" structure (*left column*). These structures display the same behavior for homogeneous initial concentrations in the immobile zones. The mobile zone is the bold box with the arrow. The size of the boxes is proportional to the porosity of the compartments. Only the vertical distance of an immobile zone to the mobile zone is to scale.

For the structures displayed on Figure 2, the effective dispersion obtained with the MRMT models converges quickly to the reference dispersion of the corresponding SINC model (Figure 5). The equivalent MRMT model with only one immobile zone (N=1), equivalent to the double porosity model [*Warren et al.*, 1963], already gives the right order of magnitude of dispersion. With N=2, the error of the MRMT model is close to10%. With N=4, it is close to 1% and with N=5, it is close to 0.1%. A very limited number of rates is thus sufficient to represent even the complex diffusive structure displayed by Figure 2d. This fundamentally comes from the homogenization nature of diffusion that systematically removes the extremes of the concentration distributions as previously noted in numerous studies [*Haggerty and Gorelick*, 1995; *Villermaux*, 1987].

In addition, the equivalent MRMT model with only one rate reproduces well the tailing of the breakthrough curve (Figure 6). As expected, introducing higher rates progressively improves the accuracy of the MRMT model at earlier times. The double peak observed for N=1 is a classical feature of double porosity models where advection is much faster than diffusion in the immobile porosity [*Michalak and Kitanidis*, 2000]. It vanishes for higher-order MRMT models (N=2 to 5), as higher rates enhance short-term mobile-immobile exchanges and remove early breakthroughs.

The quality of the MRMT model with only very few rates fundamentally comes from the dominating role of the smaller rates (i.e. larger transfer times). In fact the whole rate series as determined by the algebraic diagonalization method shows that the lowest rate dominates in every case by accounting for 70% to 85% of the total immobile porosity (Figure 7). The five lowest rates represent at least 95% of the total immobile porosity for all the studied structures. The evolution of the porosities ϕ_{im}^{i} with the rates α_i is monotonic only for the MINC model and becomes much more variable for more complex structures, highlighting the need of identification methods that do not assume any *a priori* repartition of the immobile porosity among the rates. We finally note that our results pertain to complex diffusive structures observed on a given range of scales. If not close to the mobile zone, finer details would be fast homogenized by diffusion and are unlikely to modify the identified rates. If close to the mobile zone, finer details should be treated independently in the same way as for the larger-scale structures and the MRMT models obtained at different scales should be eventually superposed.

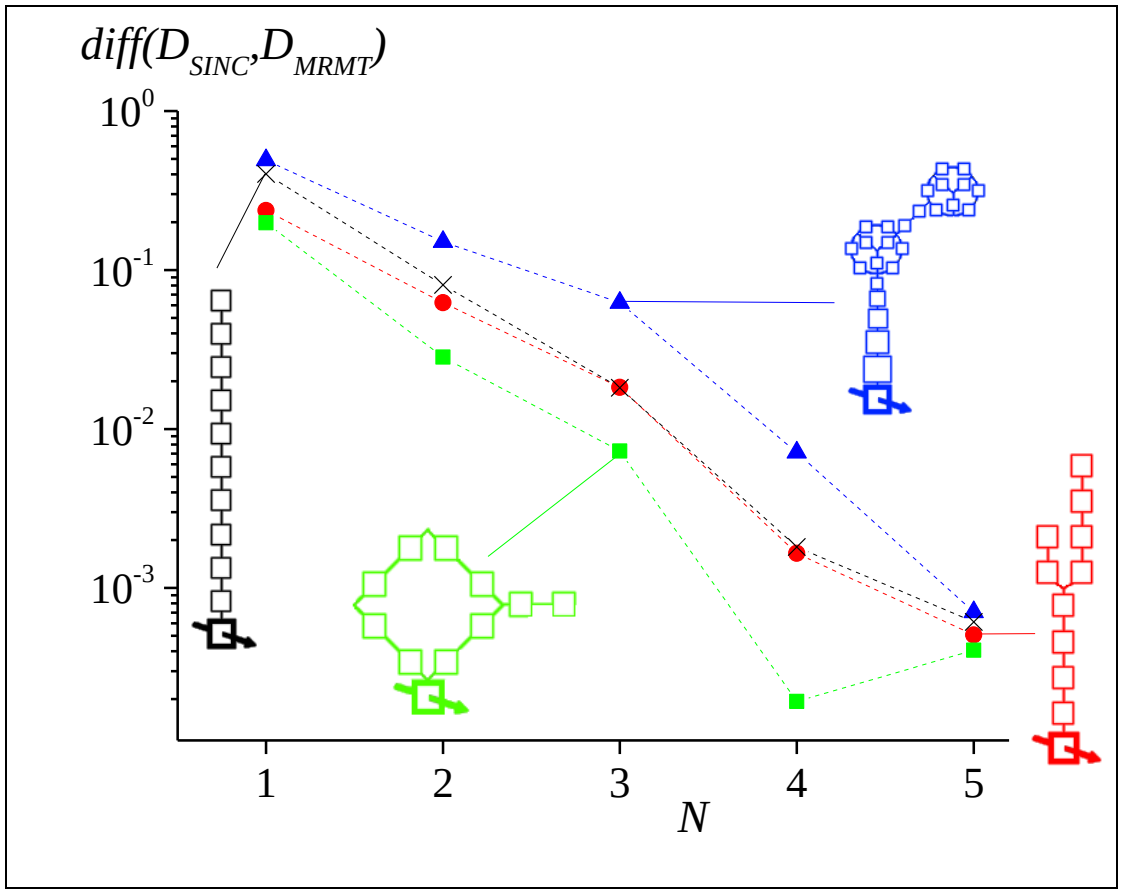

Figure 5: Differences in macrodispersions $diff\,(D_{SINC}, D_{MRMT})$ (equation (20)) between SINC models and their approximate MRMT models with a limited number of rates $N = 1 \text{ to } 5$, for the four SINC models presented in Figure 2. The determination of the approximate MRMT models is achieved with the numerical identification method in the temporal domain (Section 4.1 and *Appendix C*).

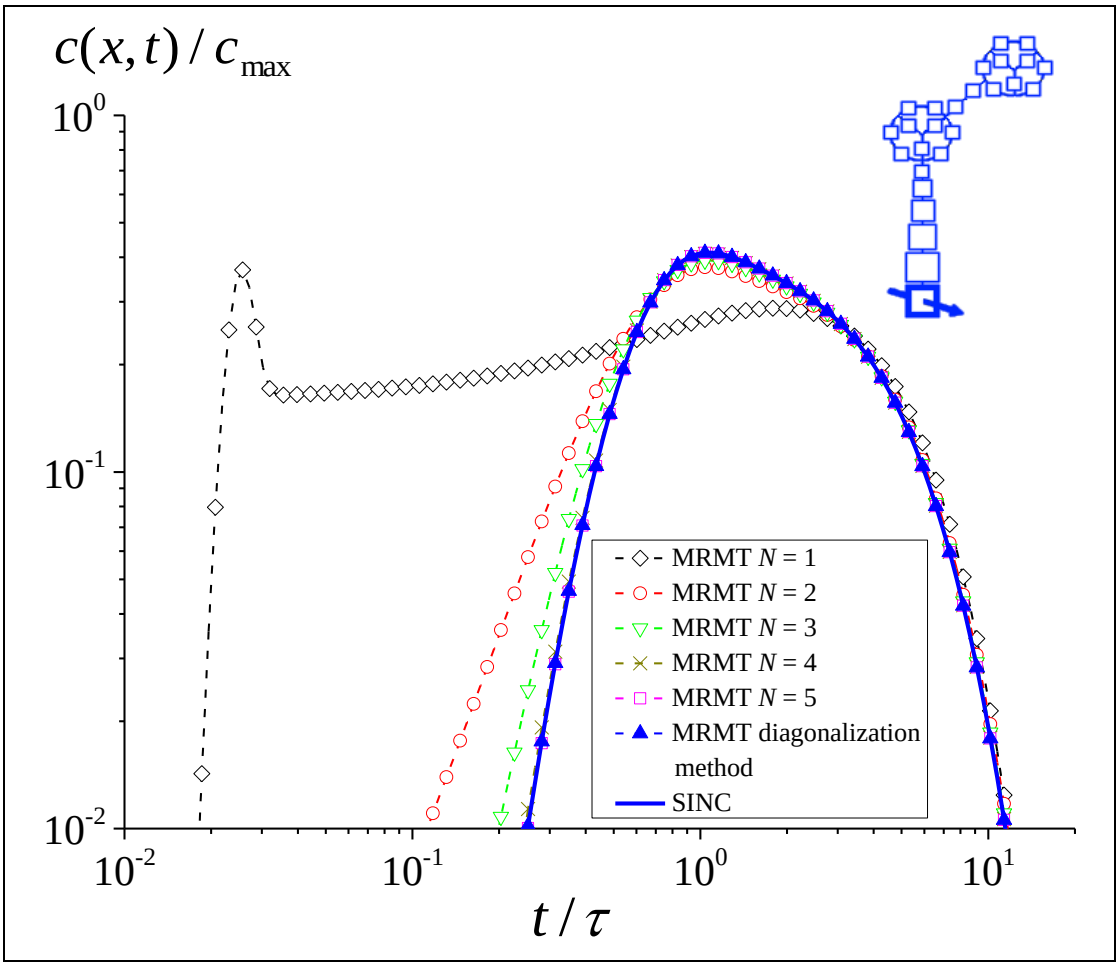

306 Figure 6: Breakthrough curves for the dissolution-like SINC model (Figure 2d) and for its
307 equivalent MRMT models, either determined by the diagonalization method (section 3), or by
308 the numerical method in the temporal domain with a limited number of N rates (Section 4.1
309 and *Appendix C*). The concentrations are measured at the position $x = 20\sigma_0$.

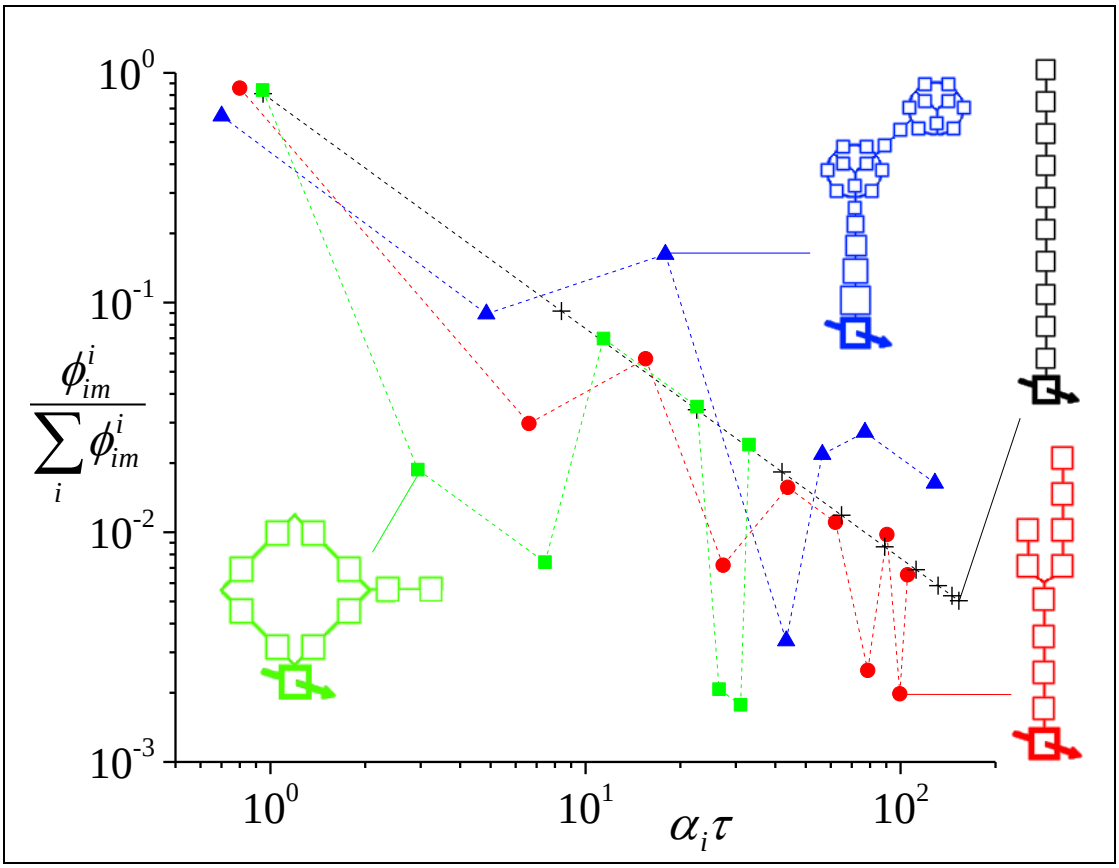

310 Figure 7: Normalized rates $\alpha_i \tau$ versus normalized porosities $\phi_{im}^i / \sum_i \phi_{im}^i$ for the MRMT

311 models equivalent to the four diffusive porosity structures presented in Figure 2, as

312 determined by the diagonalization method (section 3). Normalized rates larger than 200 or

313 corresponding to a normalized porosity smaller than 10^{-3} have been truncated. .

5 Conclusion

We define a general mobile/immobile Structured INteracting Continua (SINC) transport framework accounting for a broad variety of immobile porosity structures. Like in more classical double porosity, Multi-Rate Mass Transfer (MRMT), and Multiple INteracting Continua (MINC) frameworks, solute transport is dominated by advection in the mobile porosity and is diffusion-like in the immobile porosity. The SINC framework introduces a connectivity pattern within the immobile zone covering a broad range of diffusive geological structures including cluster of dead-end fractures, irregular matrix shapes and dissolution patterns. Immobile structures are based on branching and looping structures, and on any combination of them. Solute transport is expressed as an advection-diffusion equation coupled to algebraically defined exchanges with a finite number of immobile zones. Interactions among the immobile zones and with the mobile zone are fully determined by a simple interaction matrix, which resumes to an arrow type of matrix in the MRMT case and to a tri-diagonal matrix in the MINC case. The graph of the matrix registers the connectivity pattern while the value of its coefficients comes from relative porosities and strength of exchanges between immobile zones.

We show that any Structured INteracting Continua model is equivalent to a unique MRMT model, where the equivalence is defined as the strict identity of the concentrations in the mobile zone, whatever the initial and boundary conditions. The rates of the equivalent MRMT model are the eigenvalues of the subset of the interaction matrix where the line and column corresponding to the mobile zone are removed. The diagonalization method gives a first identification method of the equivalent MRMT with the same dimension, i.e. with the same number of immobile zones. Because of limitations coming essentially from the dimension of the immobile porosity structure, we set up alternative numerical methods designed to identify the most important rates controlling the transport of solute. Developed both in the temporal and Laplace domains, these methods seek for the combination of a finite number of exponential functions that best matches a simple discharge of the immobile zones within a quickly flushing mobile zone.

A simple sensitivity study on representative diffusive structures shows that very few rates are needed for accurately modeling the solute transport in a 1D advection-dominated mobile zone exchanging with an immobile porosity structure. Double porosity models (MRMT with a single rate) already give the right order of magnitude of macrodispersion. Differences in

346 macrodispersion drop down to around 10% for two rates, to 1% for four rates, and to less than
347 0.1% for five rates. Simplified models based on only five rates approach accurately the
348 behavior of the system at intermediate to large times and only miss the very early responses.
349 While only few rates are necessary, their distribution and associated porosities are highly
350 variable, the complexity of the structure being transferred to the identified rates and
351 associated porosities. We thus conclude that MRMT models can be very efficient for
352 modeling diffusion-like transport in a broad range of porosity structures with only very few
353 rates. Even though numerical simulations have been done in 1D mobile domains, results are
354 likely generalize to 3D. Additional simulations should also be performed to investigate the
355 behavior of mixing and chemical reactivity both between different SINC structures and
356 between the SINC structures and their simplified MRMT counterparts.

Appendix A: Diagonalization of $\hat{A}$

We show that the eigenvalues of the matrix $\hat{A}$ are real and negative and that they correspond to the opposites of the rates of the equivalent MRMT model ($-\alpha_i$). As displayed by equations (4) and (7), $\hat{A} = -\hat{\Phi}^{-1}\hat{M}$ where $\hat{\Phi} = \Phi(2\ldots N+1, 2\ldots N+1)$ and $\hat{M} = M(2\ldots N+1, 2\ldots N+1)$. $\hat{\Phi}^{-1}$ is diagonal and its diagonal elements are all positive. Thus $\hat{\Phi}^{-1}$ is positive definite, i.e. for every non-zero and real column vector *x*, $x^T\hat{\Phi}^{-1}x = \sum_i \frac{x(i)^2}{\hat{\Phi}(i,i)} > 0$. $\hat{M}$ is symmetrical, real, diagonally dominant $\left|\hat{M}(i,i)\right| \geq \sum_{j,j\neq i}\left|\hat{M}(i,j)\right|$, and strictly diagonally dominant $\left|\hat{M}(i,i)\right| > \sum_{j,j\neq i}\left|\hat{M}(i,j)\right|$ on its rows corresponding to the immobile zones connected to the mobile zone, due to the removal of the column corresponding to the mobile zone in the extraction of $\hat{A}$ from A (equation (7)). If $\hat{A}$ is additionally of rank *N*, then $\hat{A}$ is diagonalizable, has real eigenvalues, and has the same number of positive and negative eigenvalues as $-\hat{M}$ [*Horn*, 1985].

We moreover show that $-\hat{M}$ and equivalently $\hat{A}$ have strictly negative, real eigenvalues. It is the direct consequence [*Horn*, 1985] of $-\hat{M}$ being symmetrical, real, having only negative diagonal elements, and also being irreducible diagonally dominant. The diagonally dominance has been shown previously. The irreducibility property is more involved but can be proved by studying the properties of the graph defined by $\hat{M}$. When $\hat{M}$ represents an immobile structure connected to the mobile structure by a single link, at least one path exists from any immobile cell to any other immobile cell that does not cross the mobile zone, then the graph defined by $\hat{M}$ is strongly connected, so $\hat{M}$ is irreducible [*Horn*, 1985]. When several immobile zones are independently connected to the mobile zone, each of these immobile zones is associated to a strongly connected graph and to an irreducible diagonally dominant matrix, itself a sub-matrix of $\hat{M}$. The eigenvalues and eigenvectors of $\hat{M}$ are then obtained by clustering the ones of the sub-matrices.

Appendix B: Construction of the matrix *B*

The norm of each eigenvector in $\widehat{R}$ is defined up to a constant. A first straightforward step is to adjust these norms so that the sum along the 2..*N*+1 rows of *B* is equal to zero. It is achieved by taking $B_{i+1,1} = -\Lambda_i$, overly written in matrix form

$$\begin{bmatrix} B_{2,1} \\ \vdots \\ B_{N+1,1} \end{bmatrix} = -\Lambda \begin{bmatrix} 1 \\ \vdots \\ 1 \end{bmatrix}. \tag{B1}$$

Given this choice and the properties of the matrices *A* and $\widehat{R}$, we demonstrate that the sum of the elements of the first line of *B* is also zero. We express the relation between the first columns of *A* and *B* from equation (12):

$$\begin{bmatrix} B_{2,1} \\ \vdots \\ B_{N+1,1} \end{bmatrix} = \widehat{R}^{-1} \begin{bmatrix} A_{2,1} \\ \vdots \\ A_{N+1,1} \end{bmatrix}. \tag{B2}$$

As the sum of the elements of each line of *A* is zero

$$\begin{bmatrix} A_{2,1} \\ \vdots \\ A_{N+1,1} \end{bmatrix} = -\widehat{A} \begin{bmatrix} 1 \\ \vdots \\ 1 \end{bmatrix} \tag{B3}$$

equation (B2) rewrites

$$\begin{bmatrix} B_{2,1} \\ \vdots \\ B_{N+1,1} \end{bmatrix} = -\widehat{R}^{-1}\widehat{A} \begin{bmatrix} 1 \\ \vdots \\ 1 \end{bmatrix} = -\Lambda\widehat{R}^{-1} \begin{bmatrix} 1 \\ \vdots \\ 1 \end{bmatrix}. \tag{B4}$$

By substituting equation (B4) into equation (B1), we deduce that the eigenvectors comply with

$$\begin{bmatrix}1\\ \vdots\\ 1\end{bmatrix} = \widehat{R}\begin{bmatrix}1\\ \vdots\\ 1\end{bmatrix}. \tag{B5}$$

As $R^{-1}U$ corresponds to the concentrations in the equivalent model (equation (13)), equation (B5) implies that a homogeneous immobile concentration profile in SINC remains unchanged in the equivalent model. We finally express the sum of the 2...N+1 elements of the first row of B and use the result of equation(B5):

$$\begin{aligned}\sum_{j=2}^{N+1} B_{1,j} &= \begin{bmatrix}B_{1,2} & \dots & B_{1,N+1}\end{bmatrix}\begin{bmatrix}1\\ \vdots\\ 1\end{bmatrix}\\ &= \begin{bmatrix}A_{1,2} & \dots & A_{1,N+1}\end{bmatrix}\widehat{R}\begin{bmatrix}1\\ \vdots\\ 1\end{bmatrix}\\ &= \begin{bmatrix}A_{1,2} & \dots & A_{1,N+1}\end{bmatrix}\begin{bmatrix}1\\ \vdots\\ 1\end{bmatrix} = \sum_{j=2}^{N+1} A_{1,j} = -A_{1,1}\end{aligned} \tag{B6}$$

An additional condition for B to be representative of a MRMT model is $B_{1,j} > 0$ for j = 2…N+1. In the following we show that the adjustment of the norms of the eigenvectors is sufficient to ensure this condition. Equations (12) and (B2) give:

$$
\begin{aligned}
&\left[B_{1,2} \quad \dots \quad B_{1,N+1}\right] \\
&= \left[A_{1,2} \quad \dots \quad A_{1,N+1}\right]\widehat{R} \\
&= -\frac{1}{\phi_m}\left[M_{1,2} \quad \dots \quad M_{1,N+1}\right]\widehat{R} \\
&= -\frac{1}{\phi_m}\left[M_{2,1} \quad \dots \quad M_{N+1,1}\right]\widehat{R} \quad \text{because } M \text{ is symmetric} \\
&= -\frac{1}{\phi_m}\left[\phi_{im}^1 A_{2,1} \quad \dots \quad \phi_{im}^N A_{N+1,1}\right]\widehat{R} \\
&= -\frac{1}{\phi_m}\left[A_{2,1} \quad \dots \quad A_{N+1,1}\right]\begin{bmatrix}\phi_{im}^1 & & \\ & \ddots & \\ & & \phi_{im}^N\end{bmatrix}\widehat{R} \\
&= \frac{1}{\phi_m}\left[B_{2,1} \quad \dots \quad B_{N+1,1}\right]\widehat{R}^T\begin{bmatrix}\phi_{im}^1 & & \\ & \ddots & \\ & & \phi_{im}^N\end{bmatrix}\widehat{R} \qquad .
\end{aligned}
\tag{B7}
$$

We now show that the matrix $\widehat{R}^T\widehat{\Phi}\widehat{R}$ with $\widehat{\Phi} = \Phi(2\dots N+1, 2\dots N+1)$ is diagonal with only positive diagonal elements.

We note $\widehat{A} = -\widehat{\Phi}^{-1}\widehat{M}$ with $\widehat{M} = M(2\dots N+1, 2\dots N+1)$. $\widehat{M}$ is symmetric, its diagonal elements are positive, its non-zero off-diagonal elements are negative, but the sum of its elements over each of its rows is not equal to zero. As the ϕ_{im}^i are positive, we can consider the root of the matrix $\widehat{\Phi}$:

$$
\widehat{A} = \widehat{\Phi}^{-1/2}\underbrace{(-1)\widehat{\Phi}^{-1/2}\widehat{M}\widehat{\Phi}^{-1/2}}_{\widehat{C}}\widehat{\Phi}^{1/2}\,.
\tag{B8}
$$

$\widehat{C}$ is similar (in the mathematical sense) to $\widehat{A}$, so it is diagonalizable and has the same eigenvalues as $\widehat{A}$. Moreover $\widehat{C}$ is symmetric, so it can be diagonalized by an orthogonal matrix *S*:

$$
\widehat{C} = S\Lambda S^{-1}
\tag{B9}
$$

As a consequence, equation (B8) rewrites:

$$\begin{aligned} \widehat{A} &= \widehat{\Phi}^{-1/2} S \Lambda S^{-1} \widehat{\Phi}^{1/2} \\ &= \widehat{\Phi}^{-1/2} S \Lambda (\widehat{\Phi}^{-1/2} S)^{-1} \end{aligned} \quad . \tag{B10}$$

As the norms of the eigenvectors in $\widehat{R}$ are adjusted so the equation (B1) is verified, there exists a unique orthogonal matrix *S* such that

$$S = \widehat{\Phi}^{1/2} \widehat{R} \quad . \tag{B11}$$

As *S* is othogonal, $S^T S$ is diagonal with only positive diagonal elements and writes

$$S^T S = (\widehat{\Phi}^{1/2} \widehat{R})^T \widehat{\Phi}^{1/2} \widehat{R} = \widehat{R}^T \widehat{\Phi}^{1/2} \widehat{\Phi}^{1/2} \widehat{R} = \widehat{R}^T \widehat{\Phi} \widehat{R} \quad . \tag{B12}$$

The matrix $\widehat{R}^T \widehat{\Phi} \widehat{R}$, which is present in equation (B7), is thus diagonal with only positive diagonal elements. Consequently, as the $B_{1,j}$ are positive for $j = 2 \ldots N+1$, so are the $B_{j,1}$.

Appendix C: Numerical identification method of MRMT models equivalent to a SINC model

We set up an optimization scheme to get MRMT models equivalent to a SINC model. We first consider the case where the mass per unitary volume $m(t)$ discharged to an immobile zone from a flushing experiment can effectively be modeled by a series of N exponential functions with rates α_i and associate porosities ϕ_{im}^i ($m(t)=\gamma(t)$, see equation (15)). We derive a set of equivalent expressions in the Laplace domain with simple dependences on α_i and ϕ_{im}^i. We then deduce optimization strategies both in the Laplace and temporal domains.

We assume first that the SINC model is strictly equivalent to a given MRMT model as in section 2 ($m(t)=\gamma(t)$). It is the case when initial concentrations are homogeneous in the immobile zone and when the immobile zones are constantly discharging to a quickly flushed mobile zone where concentration is assumed to remain negligible ([*Haggerty and Gorelick*, 1995], Appendix B). In the Laplace domain, exponential functions become simple rational functions and $\tilde{m}(p)=\tilde{\gamma}(p)$ is expressed as

$$\tilde{m}(p)=\sum_{i=1}^{N}\frac{\phi_{im}^i c_0}{\alpha_i}\frac{1}{1+\frac{p}{\alpha_i}} \tag{C1}$$

where p is the Laplace variable and $\tilde{m}(p)$ (respectively $\tilde{\gamma}(p)$) is Laplace transform of $m(t)$ (respectively $\gamma(p)$). We multiply equation (C1) by the polynomial $P(p)$ of degree N

$$P(p)=\prod_{i=1}^{N}(1+\frac{p}{\alpha_i})=1+a_1 p+a_2 p^2+\ldots+a_N p^N \tag{C2}$$

and obtain

$$(1+a_1 p+a_2 p^2+\ldots+a_N p^N)\tilde{m}(p)=\sum_{i=1}^{N}\left[\frac{\phi_{im}^i c_0}{\alpha_i}\prod_{\substack{j=1\\ j\neq i}}^{N}(1+\frac{p}{\alpha_j})\right]. \tag{C3}$$

If we now consider the polynomial $Q_i(p)$ of degree N-1

$$Q_i(p) = \prod_{\substack{j=1 \\ j\neq i}}^{N} (1 + \frac{p}{\alpha_j}) = 1 + a_{i,1}p + a_{i,2}p^2 + \ldots + a_{i,N-1}p^{N-1} \tag{C4}$$

434 and substitute equation (C4) into equation (C3), we obtain:

$$(a_1 p + a_2 p^2 + \ldots + a_N p^N)\tilde{m}(p) + \tilde{m}(p) = \sum_{i=1}^{N} \frac{\phi_{im}^i c_0}{\alpha_i} (1 + a_{i,1}p + a_{i,2}p^2 + \ldots + a_{i,N-1}p^{N-1}) . \tag{C5}$$

435 The interest of equation (C5) is to be linear in the a_i (polynomial coefficients of $P(p)$) and in
436 ϕ_{im}^i / α_i with $i = 1 \ldots N$. We isolate these quantities from the Laplace parameter-dependant
437 elements to obtain the linear system

$$\varphi^T(p)\theta = y(p) \tag{C6}$$

438 with

$$\varphi(p) = \begin{bmatrix} p\tilde{m}(p) \\ p^2\tilde{m}(p) \\ \vdots \\ p^N\tilde{m}(p) \\ -1 \\ -p \\ \vdots \\ -p^{N-1} \end{bmatrix}, \theta = \begin{bmatrix} a_1 \\ a_2 \\ \vdots \\ a_N \\ \sum_{i=1}^{N} \frac{\phi_{im}^i c_0}{\alpha_i} \\ \sum_{i=1}^{N} \frac{\phi_{im}^i c_0}{\alpha_i} a_{i,1} \\ \vdots \\ \sum_{i=1}^{N} \frac{\phi_{im}^i c_0}{\alpha_i} a_{i,N-1} \end{bmatrix}, y(p) = -\tilde{m}(p) . \tag{C7}$$

439 Both $\varphi(p)$ and θ are vectors of dimension $2N$. The rates $-\alpha_i$ are directly obtained from the
440 roots of the polynomial $P(p)$ of equation (C2), whose coefficients are given by $\theta_1..\theta_N$. The
441 porosities ϕ_{im}^i are further deduced from $\theta_{N+1}..\theta_{2N}$ by inversing the N+1..2N equations of (C7):

$$\begin{bmatrix} \phi_{im}^1 \\ \phi_{im}^2 \\ \vdots \\ \phi_{im}^N \end{bmatrix} = G^{-1} \begin{bmatrix} \theta_{N+1} \\ \theta_{N+2} \\ \vdots \\ \theta_{2N} \end{bmatrix} \tag{C8}$$

442 with

$$G = \begin{bmatrix} c_0/\alpha_1 & \cdots & c_0/\alpha_N \\ c_0 a_{1,1}/\alpha_1 & \cdots & c_0 a_{N,1}/\alpha_N \\ \vdots & & \vdots \\ c_0 a_{1,N-1}/\alpha_1 & \cdots & c_0 a_{N,N-1}/\alpha_N \end{bmatrix} \quad \text{(C9)}$$

where the values of $a_{i,j}$ are deduced from the identified values of α_i. In the case of strict equivalence between MRMT and SINC models, the equivalent MRMT model can be found through (C6)-(C9).

In the case where MRMT and SINC models are not strictly equivalent, we seek for the composition of *N* exponential functions that best matches $\tilde{m}(p)$ on a given sampling of the Laplace parameter p_k, $k = 1,\ldots,K$ of p by using a least-square method, minimizing the mismatch objective function *J* [*Garnier et al.*, 2008; *Ljung*, 1999]:

$$J = \sum_{k=1}^{K} \left(y(p_k) - \varphi^T(p_k)\theta \right)^2 . \quad \text{(C10)}$$

The sampling should be extensive enough to contain all the information necessary to identify the different rates. If α_N is the largest rate, the initial time sampling should be smaller than $\alpha_N^{-1}/2$ following the spirit of Shannon's theorem. Adequate time sampling could then increase with time for determining the smaller rates.

The minimum $\tilde{\theta}$ of *J* is explicitly given by:

$$\tilde{\theta} = \left(\sum_{k=1}^{K} \varphi(p_k)\varphi^T(p_k) \right)^{-1} \sum_{k=1}^{K} \varphi(p_k) y(p_k) \quad \text{(C11)}$$

and the α_i and ϕ_{im}^i coefficients can be determined from the approximate $\tilde{\theta}_i$ coefficients and (C6)-(C9).

$\tilde{\theta}$ can also be obtained in the temporal domain. We first divide equation (C5) by p^N (which is equivalent to integrate *N* times over *t* in the temporal domain) because of the better numerical stability of integration compared to derivation

$$(\frac{1}{p^N}+a_1\frac{1}{p^{N-1}}+a_2\frac{1}{p^{N-2}}+...+a_N)\tilde{m}(p)=\sum_{i=1}^{N}\frac{\phi_{im}^i c_0}{\alpha_i}(\frac{1}{p^N}+a_{i,1}\frac{1}{p^{N-1}}+a_{i,2}\frac{1}{p^{N-2}}+...+a_{i,N-1}\frac{1}{p}). \quad \text{(C12)}$$

460 For convenience, we note

$$\int^{(n)} m(u)du=\int_0^t\int_0^{u_1}\int_0^{u_2}\dots\int_0^{u_{n-1}} m(u_n)du_n\dots du_2 du_1. \quad \text{(C13)}$$

461 The inverse Laplace transform of equation (C12) gives

$$\begin{aligned}&\int^{(N)} m(u)du+a_1\int^{(N-1)} m(u)du+a_2\int^{(N-2)} m(u)du+...+a_N m(t)=\\&\sum_{i=1}^{N}\frac{\phi_{im}^i c_0}{\alpha_i}(\frac{t^{N-1}}{(N-1)!}+a_{i,1}\frac{t^{N-2}}{(N-2)!}+a_{i,2}\frac{t^{N-3}}{(N-3)!}+...+a_{i,N-1})\end{aligned} \quad \text{(C14)}$$

462 As done previously in the Laplace domain, we separate the time-dependent elements from the
463 quantities depending on ϕ_{im}^i and α_i

$$\varphi(t)=\begin{bmatrix}\int^{(N-1)} m(u)du\\ \int^{(N-2)} m(u)du\\ \vdots\\ m(t)\\ -\frac{t^{N-1}}{(N-1)!}\\ -\frac{t^{N-2}}{(N-2)!}\\ \vdots\\ -1\end{bmatrix},\theta=\begin{bmatrix}a_1\\ a_2\\ \vdots\\ a_N\\ \sum_{i=1}^{N}\frac{\phi_{im}^i c_0}{\alpha_i}\\ \sum_{i=1}^{N}\frac{\phi_{im}^i c_0}{\alpha_i}a_{i,1}\\ \vdots\\ \sum_{i=1}^{N}\frac{\phi_{im}^i c_0}{\alpha_i}a_{i,N-1}\end{bmatrix},y(t)=-\int^{(N)} m(u)du. \quad \text{(C15)}$$

464 θ may also be obtained with a similar least-square method by considering a discretization of
465 time t_k (k=1...K) and by minimizing the objective function

$$J=\sum_{k=1}^{K}\left(y(t_k)-\varphi^T(t_k)\theta\right)^2. \quad \text{(C16)}$$

466 The minimum $\tilde{\theta}$ is given by

$$\tilde{\theta}=\left(\sum_{k=1}^{K}\varphi(t_k)\varphi^T(t_k)\right)^{-1}\sum_{k=1}^{K}\varphi(t_k)y(t_k). \quad \text{(C17)}$$

Appendix D: Application of the numerical identification method to cases $N=1$ and $N=2$

We recall the expression of the discharge of one immobile zone in MRMT model into a mobile zone of constant concentration zero (equation (C1)):

$$m(t) = \sum_{i=1}^{N} c_0 \phi_{im}^i \exp(-\alpha_i t) \tag{D1}$$

where $m(t)$ is the remaining mass per unitary volume of solute and c_0 is the initial homogeneous immobile concentration.

Case $N=1$

In Laplace domain, equation (D1) rewrites:

$$\tilde{m}(p) = \frac{\phi_{im}^1 c_0}{\alpha_1} \frac{1}{1+\frac{p}{\alpha_1}} \tag{D2}$$

$$(1+\frac{p}{\alpha_1})\tilde{m}(p) = \frac{\phi_{im}^1 c_0}{\alpha_1} \tag{D3}$$

Dividing equation (D3) by p and then using the inverse Laplace transform, we obtain:

$$\int_0^t m(u)du + \frac{m(t)}{\alpha_1} = \frac{\phi_{im}^1 c_0}{\alpha_1} \tag{D4}$$

Equations (D3) and (D4) are both linear in quantities depending on the unknown parameters α_1 and ϕ_{im}^1 to be identified. Equation (D4) can be written under the form:

$$\varphi^T(t)\theta = y(t) \tag{D5}$$

with:

$$\varphi(t) = \begin{bmatrix} m(t) \\ -1 \end{bmatrix},\ \theta = \begin{bmatrix} 1/\alpha_1 \\ c_0\phi_{im}^1/\alpha_1 \end{bmatrix},\ y(t) = -\int_0^t m(u)du\ . \tag{D6}$$

The vector $\tilde{\theta}$ which minimize the quantity:

$$J = \sum_{k=1}^{K} \left(y(t_k) - \varphi^T(t_k)\theta \right)^2 \tag{D7}$$

with a discretization t_k, $k = 1,...,K$ of t, is given by:

$$\tilde{\theta} = \left(\sum_{k=1}^{K} \varphi(t_k)\varphi^T(t_k) \right)^{-1} \sum_{k=1}^{K} \varphi(t_k) y(t_k) \tag{D8}$$

where

$$\varphi(t_k)\varphi^T(t_k) = \begin{bmatrix} m(t_k)^2 & -m(t_k) \\ -m(t_k) & 1 \end{bmatrix}, \quad \varphi(t_k) y(t_k) = \begin{bmatrix} -m(t_k) \int_0^{t_k} m(u)du \\ \int_0^{t_k} m(u)du \end{bmatrix} \tag{D9}$$

so

$$\tilde{\theta} = \begin{bmatrix} \sum_{k=1}^{K} m(t_k)^2 & -\sum_{k=1}^{K} m(t_k) \\ -\sum_{k=1}^{K} m(t_k) & K \end{bmatrix}^{-1} \begin{bmatrix} -\sum_{k=1}^{K} m(t_k) \int_0^{t_k} m(u)du \\ \sum_{k=1}^{K} \int_0^{t_k} m(u)du \end{bmatrix}. \tag{D10}$$

We then get α_1 and ϕ_{im}^1:

$$\alpha_1 = \frac{1}{\tilde{\theta}_1} \quad , \quad \phi_{im}^1 = \frac{\tilde{\theta}_2 \alpha_1}{c_0}. \tag{D11}$$

Case $N = 2$

In Laplace domain, equation (D1) rewrites:

$$\tilde{m}(p) = \frac{\phi_{im}^1 c_0}{\alpha_1} \frac{1}{1 + \frac{p}{\alpha_1}} + \frac{\phi_{im}^2 c_0}{\alpha_2} \frac{1}{1 + \frac{p}{\alpha_2}} \tag{D12}$$

which gives when multiplied by $(1 + p/\alpha_1)(1 + p/\alpha_2)$

$$(1 + p/\alpha_1)(1 + p/\alpha_2)\tilde{m}(p) = \frac{\phi_{im}^1 c_0}{\alpha_1}(1 + p/\alpha_2) + \frac{\phi_{im}^2 c_0}{\alpha_2}(1 + p/\alpha_1). \tag{D13}$$

487 We divide then equation (D13) by p^2 (which is equivalent to integrate two times over t)

$$\frac{1}{\alpha_1\alpha_2}\tilde{m}(p)+(\frac{1}{\alpha_1}+\frac{1}{\alpha_2})\frac{\tilde{m}(p)}{p}+\frac{\tilde{m}(p)}{p^2}=\frac{\phi_{im}^1 c_0}{\alpha_1}(\frac{1}{p^2}+\frac{1}{p\alpha_2})+\frac{\phi_{im}^2 c_0}{\alpha_2}(\frac{1}{p^2}+\frac{1}{p\alpha_1}). \qquad \text{(D14)}$$

488 Then, by using the inverse Laplace transform, we obtain:

$$\frac{1}{\alpha_1\alpha_2}m(t)+(\frac{1}{\alpha_1}+\frac{1}{\alpha_2})\int_0^t m(u)du+\int_0^t\int_0^u m(v)dvdu=\frac{\phi_{im}^1 c_0}{\alpha_1}(t+\frac{1}{\alpha_2})+\frac{\phi_{im}^2 c_0}{\alpha_2}(t+\frac{1}{\alpha_1}). \qquad \text{(D15)}$$

489 Again equations (D12) and (D13) are both linear in quantities depending on the unknown
490 parameters α_i and ϕ_{im}^i to be identified. Equation (D15) and can be written under the form:

$$\varphi^T(t)\theta=y(t) \qquad \text{(D16)}$$

491 with:

$$\varphi(t)=\begin{bmatrix}\int_0^t m(u)du\\ m(t)\\ -t\\ -1\end{bmatrix},\ \theta=\begin{bmatrix}1/\alpha_1+1/\alpha_2\\ 1/(\alpha_1\alpha_2)\\ \frac{\phi_{im}^1 c_0}{\alpha_1}+\frac{\phi_{im}^2 c_0}{\alpha_2}\\ \frac{\phi_{im}^1 c_0}{\alpha_1\alpha_2}+\frac{\phi_{im}^2 c_0}{\alpha_1\alpha_2}\end{bmatrix},\ y(t)=-\int_0^t\int_0^u m(v)dvdu\,. \qquad \text{(D17)}$$

492 The vector $\tilde{\theta}$ which minimizes the quantity:

$$J=\sum_{k=1}^{K}\left(y(t)-\varphi^T(t)\theta\right)^2 \qquad \text{(D18)}$$

493 with a discretization t_k, $k=1,...,K$ of t, is given by:

$$\tilde{\theta}=\left(\sum_{k=1}^{K}\varphi(t_k)\varphi^T(t_k)\right)^{-1}\sum_{k=1}^{K}\varphi(t_k)y(t_k)\,. \qquad \text{(D19)}$$

494 We then have the following relations:

$$\begin{cases} 1/\alpha_1 + 1/\alpha_2 &= \tilde{\theta}_1 \\ 1/(\alpha_1\alpha_2) &= \tilde{\theta}_2 \\ \dfrac{\phi_{im}^1 c_0}{\alpha_1} + \dfrac{\phi_{im}^2 c_0}{\alpha_2} &= \tilde{\theta}_3 \\ \dfrac{\phi_{im}^1 c_0}{\alpha_1\alpha_2} + \dfrac{\phi_{im}^2 c_0}{\alpha_1\alpha_2} &= \tilde{\theta}_4 \end{cases} \tag{D20}$$

from which we can identify the unknown parameters $-\alpha_1$ and $-\alpha_2$ may be obtained as the roots of the polynomial $1+\tilde{\theta}_1 x+\tilde{\theta}_2 x^2$. Once α_1 and α_2 are identified, ϕ_{im}^1 and ϕ_{im}^2 are given by:

$$\begin{bmatrix} \phi_{im}^1 \\ \phi_{im}^2 \end{bmatrix} = \frac{1}{c_0}\begin{bmatrix} 1/\alpha_1 & 1/\alpha_2 \\ 1/\alpha_1\alpha_2 & 1/\alpha_1\alpha_2 \end{bmatrix}^{-1}\begin{bmatrix} \tilde{\theta}_3 \\ \tilde{\theta}_4 \end{bmatrix}. \tag{D21}$$

Acknowledgements

The ANR is acknowledged for its funding through its project H2MNO4 under the number ANR-12-MONU-0012-01. The authors are also grateful to Linda Luquot, Alain Rapaport and Jesús Carrera for stimulating discussions, and additionally to Linda Luquot for providing the illustrative dissolution patterns. We also thank the four anonymous reviewers for their insightful and critical review of the manuscript, as well as Cass Miller for his editorial work.

References

Benson, D. A., and M. M. Meerschaert (2009), A simple and efficient random walk solution of multi-rate mobile/immobile mass transport equations, *Advances in Water Resources*, *32*(4), 532-539, doi:http://dx.doi.org/10.1016/j.advwatres.2009.01.002.

Benson, D. A., R. Schumer, M. M. Meerschaert, and S. W. Wheatcraft (2001), Fractional dispersion, Lévy motion, and the MADE tracer test, *Transport in Porous Media*, *42*(1-2), 211-240, doi:10.1007/978-94-017-1278-1_11.

Benson, D. A., S. W. Wheatcraft, and M. M. Meerschaert (2000), Application of a fractional advection-dispersion equation, *Water Resources Research*, *36*(6), doi:http://dx.doi.org/10.1029/2000WR900031.

Berkowitz, B., A. Cortis, M. Dentz, and H. Scher (2006), Modeling non-Fickian transport in geological formations as a continuous time random walk, *Reviews of Geophysics*, *44*(2), doi:10.1029/2005rg000178.

Berkowitz, B., and H. Scher (1998), Theory of anomalous chemical transport in random fracture networks, *Physical Review E*, *57*(5), doi:http://dx.doi.org/10.1103/PhysRevE.57.5858.

Berkowitz, B., H. Scher, and S. Silliman (2000), Anomalous transport in laboratory-scale, heterogeneous porous media, *Water Resources Research*, *36*(1), doi:http://dx.doi.org/10.1029/1999WR900295.

Carrera, J., X. Sánchez-Vila, I. Benet, A. Medina, G. Galarza, and J. Guimerà (1998), On matrix diffusion: formulations, solution methods and qualitative effects, *Hydrogeology Journal*, *6*(1), doi:http://dx.doi.org/10.1007/s100400050143.

Cushman, J. H., and T. R. Ginn (2000), Fractional advection-dispersion equation: A classical mass balance with convolution-Fickian flux, *Water Resources Research*, *36*(12), doi:http://dx.doi.org/10.1029/2000WR900261.

de Dreuzy, J. R., A. Rapaport, T. Babey, and J. Harmand (2013), Influence of porosity structures on mixing-induced reactivity at chemical equilibrium in mobile/immobile Multi-Rate Mass Transfer (MRMT) and Multiple INteracting Continua (MINC) models, *Water Resources Research*, *49*(12), 8511-8530, doi:10.1002/2013WR013808.

Dentz, M., and B. Berkowitz (2003), Transport behavior of a passive solute in continuous time random walks and multirate mass transfer, *Water Resources Research*, *39*(5), 1111, doi:10.1029/2001WR001163.

Dentz, M., A. Cortis, H. Scher, and B. Berkowitz (2004), Time behavior of solute transport in heterogeneous media: transition from anomalous to normal transport, *Advances in Water Resources*, *27*(2), 155-173, doi:http://dx.doi.org/10.1016/j.advwatres.2003.11.002.

Fernandez-Garcia, D., G. Llerar-Meza, and J. J. Gomez-Hernandez (2009), Upscaling transport with mass transfer models: Mean behavior and propagation of uncertainty, *Water Resources Research*, *45*, doi:10.1029/2009wr007764.

Flekkøy, E. G., A. Malthe-Sørenssen, and B. Jamtveit (2002), Modeling hydrofracture, *J. Geophys. Res.*, *107*(B8), 2151.

Garnier, H., L. Wang, and P. Young (2008), Direct Identification of Continuous-time Models from Sampled Data: Issues, Basic Solutions and Relevance, in *Identification of Continuous-time Models from Sampled Data*, edited by H. Garnier and L. Wang, pp. 1-29, Springer London, doi:10.1007/978-1-84800-161-9_1.

Golfier, F., M. Quintard, F. Cherblanc, B. A. Zinn, and B. D. Wood (2007), Comparison of theory and experiment for solute transport in highly heterogeneous porous medium, *Advances in Water Resources*, *30*(11), 2235-2261, doi:10.1016/j.advwatres.2007.05.004.

Golfier, F., C. Zarcone, B. Bazin, R. Lenormand, D. Lasseux, and M. Quintard (2002), On the ability of a Darcy-scale model to capture wormhole formation during the dissolution of a porous medium, *Journal of Fluid Mechanics*, *457*, 213-254, doi:10.1017/s0022112002007735.

Gotovac, H., V. Cvetkovic, and R. Andricevic (2009), Flow and travel time statistics in highly heterogeneous porous media, *Water Resources Research*, *45*, 24, doi:http://dx.doi.org/10.1029/2008WR007168.

Gouze, P., Y. Melean, T. Le Borgne, M. Dentz, and J. Carrera (2008), Non-Fickian dispersion in porous media explained by heterogeneous microscale matrix diffusion, *Water Resources Research*, *44*(11), 19, doi:http://dx.doi.org/10.1029/2007wr006690.

Haggerty, R. (2001), Matrix diffusion - heavy-tailed residence time distributions and their influence on radionuclide retention, paper presented at 5th GEOTRAP Workshop on Radionuclide Retention in Geologic Media,May 7-9, 2001, Organisation for Economic Co-Operation and Development, Nuclear Energy Agency, 75 - Paris (France), Oskarshamn, Sweden, 2002.

Haggerty, R., S. W. Fleming, L. C. Meigs, and S. A. McKenna (2001), Tracer tests in a fractured dolomite 2. Analysis of mass transfer in single-well injection-withdrawal tests, *Water Resources Research*, *37*(5), doi:http://dx.doi.org/10.1029/2000WR900334.

Haggerty, R., and S. M. Gorelick (1995), Multiple-Rate Mass Transfer for Modeling Diffusion and Surface Reactions in Media with Pore-Scale Heterogeneity, *Water Resources Research*, *31*(10), 2383-2400, doi:10.1029/95WR10583.

Haggerty, R., C. F. Harvey, C. F. von Schwerin, and L. C. Meigs (2004), What controls the apparent timescale of solute mass transfer in aquifers and soils? A comparison of experimental results, *Water Resources Research*, *40*(1), doi:10.1029/2002wr001716.

Haggerty, R., S. A. McKenna, and L. C. Meigs (2000), On the late-time behavior of tracer test breakthrough curves, *Water Resources Research*, *36*(12), 3467-3479, doi:http://dx.doi.org/10.1029/2000WR900214.

Horn, R. A. (1985), *Matrix analysis / Roger A. Horn, Charles R. Johnson*, Cambridge University Press, Cambridge ; New York.

Jardine, P. M., W. E. Sanford, J. P. Gwo, O. C. Reedy, D. S. Hicks, J. S. Riggs, and W. B. Bailey (1999), Quantifying diffusive mass transfer in fractured shale bedrock, *Water Resources Research*, *35*(7), 2015-2030, doi:10.1029/1999WR900043.

Karimi-Fard, M., B. Gong, and L. J. Durlofsky (2006), Generation of coarse-scale continuum flow models from detailed fracture characterizations, *Water Resources Research*, *42*(10), doi:http://dx.doi.org/10.1029/2006WR005015.

Ljung, L. (1999), *System identification : theory for the user*, Prentice Hall, Upper Saddle River.

Luquot, L., O. Rodriguez, and P. Gouze (2014), Experimental Characterization of Porosity Structure and Transport Property Changes in Limestone Undergoing Different Dissolution Regimes, *Transp Porous Med*, *101*(3), 507-532, doi:10.1007/s11242-013-0257-4.

Michalak, A. M., and P. K. Kitanidis (2000), Macroscopic behavior and random-walk particle tracking of kinetically sorbing solutes, *Water Resources Research*, *36*(8), 2133-2146, doi:10.1029/2000wr900109.

Neretnieks, I. (1980), Diffusion in the Rock Matrix: An Important Factor in Radionucleside Retardation?, *Journal of Geophysical Research*, *85*(B8), 4379-4397, doi:http://dx.doi.org/10.1029/JB085iB08p04379.

Neuman, S. P., and D. M. Tartakovsky (2009), Perspective on theories of non-Fickian transport in heterogeneous media, *Advances in Water Resources*, *32*(5), 670-680, doi:10.1016/j.advwatres.2008.08.005.

Noetinger, B., and T. Estebenet (2000), Up-scaling of double porosity fractured media using continuous-time random walks methods, *Transport in Porous Media*, *39*(3).

Pruess, K. (1992), Brief Guide to the MINC - Method for Modeling Flow and Transport in Fractured Media*Rep.*, Earth Sciences Division, Lawrence Berkeley National Laboratory. Berkeley CA USA.

Pruess, K., and T. N. Narasimhan (1985), A practical method for modeling fluid and heat-flow in fractured porous-media, *Society of Petroleum Engineers Journal*, *25*(1), 14-26, doi:http://dx.doi.org/10.2118/10509-PA.

Silva, O., J. Carrera, M. Dentz, S. Kumar, A. Alcolea, and M. Willmann (2009), A general real-time formulation for multi-rate mass transfer problems, *Hydrology and Earth System Sciences*, *13*(8), 1399-1411, doi:http://dx.doi.org/10.5194/hess-13-1399-2009.

Sornette, A., P. Davy, and D. Sornette (1993), Fault Growth in Brittle-Ductile Experiments and the Mechanics of Continental Collisions, *Journal of Geophysical Research-Solid Earth*, *98*(B7), 12111-12139, doi:http://dx.doi.org/10.1029/92JB01740.

Sudicky, E. A., and E. O. Frind (1982), Contaminant transport in fractured porous-media - analytical solutions for a system of parallel fractures, *Water Resources Research*, *18*(6), 1634-1642, doi:http://dx.doi.org/10.1029/WR018i006p01634.

Tang, D. H., E. O. Frind, and E. A. Sudicky (1981), Contaminant transport in fractured porous-media - analytical solution for a single fracture, *Water Resources Research*, *17*(3), 555-564, doi:http://dx.doi.org/10.1029/WR017i003p00555.

Tsang, Y. W. (1995), Study of alternative tracer tests in characterizing transport in fractured rocks, *Geophysical Research Letters*, *22*(11), 1421-1424, doi:10.1029/95GL01093.

Villermaux, J. (1987), Chemical-engineering approach to dynamic modeling of linear chromatography - a flexible method for representing complex phenomena from simple concepts, *Journal of Chromatography*, *406*, 11-26, doi:10.1016/s0021-9673(00)94014-7.

Warren, J. E., P. J. Root, and M. Aime (1963), The Behavior of Naturally Fractured Reservoirs, *Society of Petroleum Engineers Journal*, *September*, 245-255, doi:http://dx.doi.org/10.2118/426-PA.

Willmann, M., J. Carrera, and X. Sanchez-Vila (2008), Transport upscaling in heterogeneous aquifers: What physical parameters control memory functions?, *Water Resources Research*, *44*(12), doi:10.1029/2007wr006531.

Figure captions

Figure 1: (a) Skeleton of a dissolution feature in an oolitic limestone, observed by X-ray micro-tomography [*Luquot et al.*, 2014]. The dissolving acidic solution percolates from top to bottom on the general view (bottom left). Its pH increases from top to bottom and from inside out of the main flow path indicated by the curved arrow on the detailed view (top right). The acid dissolves preferentially the calcite cement surrounding the oolites, the size of the pores progressively decreases away from the main flow path, and the organization of the pores becomes more complex. (b) Structured INteracting Continua model (SINC) sketched from the dissolution pattern of (a) with three cross sections transversal to the mobile zone materialized by the arrow. (c) Equivalent MRMT model with the 5 most important rates as determined by the numerical methods set up in section 4. The size of the boxes scales with the porosity affected to the rates labeled by triangles in Figure 7.

Figure 2: Examples of Structured INteracting Continua (SINC) used to illustrate and validate the numerical identification methods of the equivalent MRMT models. From left to right, the diffusive porosity structures are (a) the classical Multiple INteracting Continua (MINC) [*Pruess and Narasimhan*, 1985], (b) an asymmetric Y with a single junction, (c) an asymmetric loop, and (d) the dissolution structure presented in Figure 1. The size of the immobile cells is proportional to their porosity and the distance along the immobile structure is to scale. The mobile zone is represented by the thick black box with the crossing arrow. Its size has been exaggerated 10 times to be clearly marked. To be comparable, the four structures have the same total porous volume and the same radius of gyration taken with respect to the mobile zone.

Figure 3: Diffusive porosity structures represented as cross-sections transversal to the mobile zone direction ((a),(b)), with their associated interaction matrix A ((c),(d)) for the asymmetric Y (*top*) and MRMT structures (*bottom*). Dotted frames around subsets of the immobile porosity structures ((a) and (b)) and around matrix lines ((c) and (d)) show how structures are translated in matrix form. Parameters for the asymmetric Y structure are taken from Table 1 and the multiplicative factor η (η=5.015) is equal to the ratio of the distance between two consecutive immobile zones to the radius of gyration of the immobile domain to the mobile zone. β is the ratio of the total immobile porosity to the mobile porosity.

Figure 4: Diffusive porosity structures used to check the numerical implementation of the SINC model, equivalent to the "MINC 1D" structure (*left column*). These structures display the same behavior for homogeneous initial concentrations in the immobile zones. The mobile zone is the bold box with the arrow. The size of the boxes is proportional to the porosity of the compartments. Only the vertical distance of an immobile zone to the mobile zone is to scale.

Figure 5: Differences in macrodispersions $diff\,(D_{SINC}, D_{MRMT})$ (equation (20)) between SINC models and their approximate MRMT models with a limited number of rates $N = 1 \text{ to } 5$, for the four SINC models presented in Figure 2. The determination of the approximate MRMT models is achieved with the numerical identification method in the temporal domain (Section 4.1 and *Appendix C*).

Figure 6: Breakthrough curves for the dissolution-like SINC model (Figure 2d) and for its equivalent MRMT models, either determined by the diagonalization method (section 3), or by the numerical method in the temporal domain with a limited number of *N* rates (Section 4.1 and *Appendix C*). The concentrations are measured at the position $x = 20\sigma_0$.

Figure 7: Normalized rates $\alpha_i \tau$ versus normalized porosities $\phi_{im}^i / \sum_i \phi_{im}^i$ for the MRMT models equivalent to the four diffusive porosity structures presented in Figure 2, as determined by the diagonalization method (section 3). Normalized rates larger than 200 or corresponding to a normalized porosity smaller than 10^{-3} have been truncated. .